Scientific Progress in China's Lunar Exploration Program

AUTHORS

XU Lin
OUYANG Ziyuan

Key Laboratory of Lunar and Deep Space Exploration, National Astronomical Observatories, Chinese Academy of Sciences, Beijing 100012

ABSTRACT

Chang'E-1, the first lunar mission in China, was successfully launched on October 24, 2007, which opened the prelude of China's Lunar Exploration Program. Later on, the Chang'E-2 and Chang'E-3 satellites were successfully launched in 2010 and 2013, respectively. In order to achieve the science objectives, various payloads boarded the spacecraft. The scientific data from these instruments were received by Beijing and Kunming ground stations simultaneously. Up to now, about 5.628 Terabytes of raw data were received totally. A series of research results has been achieved. This paper presents a brief introduction to the main scientific results and latest progress from Chang'E-3 mission.

KEY WORDS

China's Lunar Exploration Program, Chang'E satellite, Scientific result, Moon

1 Introduction

China's Lunar Exploration Program (CLEP) was also named as Chang'E mission, which is divided into three phases named by "circling around the moon", "landing on the moon" and "returning from the moon". The main task of these lunar exploration stages is to carry out lunar exploration by means of unmanned spacecraft before 2020. The first stage of CLEP (circling around the moon) was accomplished by Chang'E-1, which made a breakthrough in the development of key technology of lunar orbiting exploration, and conducted a global, integral and synthetic exploration on the lunar topography, lunar surface chemical composition, lunar soil characteristic features and Earth-lunar space environment. The second phase of China's lunar exploration program (landing on the moon) includes Chang'E-2, Chang'E-3 and Chang'E-4 missions, the main task of which is to carry out experiments on soft landing and lunar vehicle technique, scientific detections such as lunar local geological in-situ measurements, astronomical observation and mapping the Earth's plasmasphere. The third phase of China lunar exploration program (returning) includes Chang'E-5 and Chang'E-6

missions, the main task of which is to launch the automatic lunar surface sample collector, collect lunar rock and soil samples, and return them back to the Earth. China is expected to launch Chang'E-5 in 2017.

Chang'E-1 satellite was the first lunar probe in China, which was launched at 10:05 GMT on October 24, 2007 at the Xichang Satellite Launch Center in Southwest China, and crashed on the surface of the Moon under control at 16:13 GMT on March 1, 2009. The impact point was located at 52.36°E, 1.50°S, in the north of Mare Fecunditatis. In fact, Chang'E-2 orbiter was the backup of Chang'E-1 satellite of Phase one, after the success of Chang'E-1 mission, it became a technical test orbiter of Chang'E-3 probe and was launched at 18:59 GMT on October 1, 2010 at the Xichang Satellite Launch Center in Southwest China, with a designed life till April 1, 2011. After the pre-designed plan was accomplished successfully, the spacecraft conducted an extended mission to perform a transfer to the Earth-Sun L_2 Lagrangian point 1500000 kilometers away from the Earth on August 25, 2011, for testing the tracking equipment and demonstrating the operation of deep space missions. On April 15, 2012, Chang'E-2 left from the L_2 and headed for a close flyby of asteroid Toutatis with the serial number of 4179. At a distance of about 3.2 kilometers to the asteroid, the images of Toutatis with a resolution 10 m was obtained.

Chang'E-3 probe is the third robotic lunar mission of CLEP, which consists of a lander and a rover (Yutu, or Jade Rabbit). It was successfully launched at 13:30 on December 2, 2013 at the Xichang Satellite Launch Center in Southwest China and on December 14, 2013 successfully soft-landed in the predicted site east of Sinus Iridum of the Moon. Its main scientific goals include investigating the lunar local surface topography, geological structure and chemical compositions, mapping Earth's plasmasphere by using the ultraviolet camera onboard the lander, and monitoring variable stars, bright active galactic nuclei by a Moon-based telescope onboard the lander.

2 New Progress in China's Lunar Exploration Program

2.1 Main Results and Progress by Chang'E-1 and Chang'E-2

Eight sets of scientific instruments were chosen as payloads on Chang'E-1 lunar orbiter, including CCD stereo camera (CCD), Imaging Interferometer (IIM), Laser Altimeter (LAM), Microwave Radiometer(MRM), Gamma-Ray Spectrometer (GRS), X-Ray Spectrometer (XRS), High-energy Particle Detector (HPD), and Solar Wind Ion Detector (SWID). A total of 1.37 TB data were obtained from these instruments onboard Chang'E-1.

Compared to Chang'E-1, besides some technical test tasks, the resolution of stereo camera changed from 120 m to 7 m, and one of the scientific payloads "IIM" was cancelled, the scientific objectives and other seven scientific payloads are the same as those on the Chang'E-1 orbiter. A total of 3.5 TB data were obtained from these instruments onboard Chang'E-2.

The main science results derived from Chang'E-1 and Chang'E-2 were concluded as follows.

2.1.1 Data from CCD Stereo Camera and Laser Altimeter

By way of combination of the CCD stereo camera with the laser altimeter, Chang'E-1 accomplished the drawing of China's first global image and the first three-dimensional image of the lunar surface. In addition, using image data, plane and 3D topography maps of some important lunar geologic site image, *e.g.* the global DEM images with a resolution of 3 km were obtained.

Chang'E-2 has made a new breakthrough in developing the key technology for lunar surface dimensional image data processing, as manifested by the drawing of global image of the Moon with the resolution of 7 m. This is the top-level fully global image of the Moon obtained at present time. Additionally, the high-definition image of Sinus Iridum on the Moon with a resolution of 1 m, where Chang'E-3 will land, was shot. In addition, the precise topographic and geomorphic data for the landing zone were provided. By making use of the image data and LRO laser altitude data provided by Chang'E-2, a precise lunar altitude model with a spatial resolution of 20 m was established [1].

2.1.2 The First Microwave Detection of the Moon

The microwave radiometer was firstly used to detect fully lunar microwave activities from the lunar orbit throughout the world. Chang'E-1 (in 200 km orbit) and Chang'E-2 (in 100 km orbit) firstly obtained the world microwave brightness temperature map on a global scale with the frequencies of 3 GHz, 7.8 GHz, 19.35 GHz and 37 GHz and established the Microwave Moon (MicM) [2]. An hour angle as lunar local time was defined, rather than lunar phase and UTC time. The Brightness Temperature (TB) data observed at different

lunar local time, were normalized into the TB at the same lunar local time by the regression method. Using the normalized TB data, we have got the first microwave maps of the complete Moon at the highest resolution. On the nighttime microwave maps, we discovered hundreds of cold spots on the lunar surface (see Figure 1) [3]. However, most of the spots are shown as hot spots in the LRO diviner's infrared observation. The correlations between the cold spots and their geological characteristics were analyzed. It is found that most of the cold spots are located in the young craters. It is suggested that the high rock abundance and different thermal properties are responsible for the abnormal thermal behavior. Using the three-layer model we explained the characteristics of microwave thermal emission on the lunar surface and inversed the distribution of lunar soil thickness. In this model the influence of $FeO+TiO_2$ on the model was taken into consideration, thus making the results more reliable [4]. By analyzing the microwave brightness temperature data of lunar soil for different frequency bands, it was found that there exist brightness temperature abnormal zones in lunar maria [5].

By analyzing Chang'E-2 microwave data on lunar surface impact crater size, slope, filling and elevation, it was found that the microwave brightness temperature profile of the impact craters is related to their shape [6]. Lunar microwave radiation possesses regular ring texture, *i.e.*, showing zonal distribution, with the brightness temperature tending to decrease from the equator to the South Pole. From the analysis it is held that the lunar soil temperature gradient in the Moon's poles is smaller than that in the other areas. The variation of microwave brightness temperature tends to become synchronous with elevation beyond -85^{o} latitude. It was also found that there exist brightness temperature zones in the impact craters in the south poles of the Moon. Those zones may represent the shallow zones, and water ice may be deposited in those zones [7]. The microwave radiation data at 19 GHz and 37 GHz were used for inversion to obtain the data on the distribution and variation of temperatures of lunar soil and regolith layers in different time periods of lunar day and lunar night in the region of Sinus Iridum. It is thought that the temperature variation of lunar soil is greater than that of lunar regolith [8].

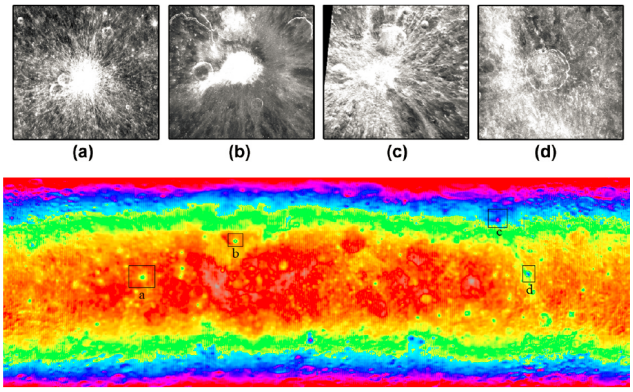

Fig.1 Some typical cold spots found on the nighttime microwave map observed at 37 GHz frequency channels by Chang'E-1 microwave radiometer. (a) Crater Lents. (b) Crater Aristarchus. (c) Crater Giordano Bruno. (d) Crater King. The crater images were photographed by Chang'E-1 CCD stereo camera. All these craters have bright rays and are much younger than the surrounding surface

2.1.3 Inversion of Lunar Soil Thickness and Estimation of ^{3}He Abundance

On the basis of the actually measured microwave brightness temperature data, the distribution map of fully lunar soil thickness was established through inversion. As the Chang'E LMS results were obtained through actual measurement on lunar surface from the lunar orbit for the first time throughout the world, as compared to the results obtained in the past, the results are much closer to the actual values. Research results showed that the lunar regolith depth is within the range of 4–6 m on average. The regolith thickness in lunar mare is relatively small while that in lunar land areas is relatively large. But in the middle-latitude areas the regolith thickness of lunar land surface is 7.6 m on average. It was also estimated that the regions with the regolith thickness being more than 5 m account for 43% of lunar surface. This result indicated that the thickness is a bit smaller than the originally estimated thickness. The inversed results were also compared with the actually estimated results from the Apollo landing site and the radar detected results from the lunar basement[2,4,9]. The lunar regolith thickness was used for the first time in the world to estimate the ^{3}He resource volume. In this way the ^{3}He reserves of the whole Moon were more precisely estimated to be about 1030000 ton[2]and 1290000 ton[10]. Also, some scholars estimated the total lunar regolith ^{3}He reserves to be 6.6×10^8 kg. The ^{3}He contents of regolith layers in the nearside of the Moon is 3.7×10^8 kg, while those in the farside are 2.9×10^8 kg[9].

2.1.4 Chemical and Mineral Compositions of Lunar Surface

By inversion on the basis of the Chang'E-1 IIM data, we obtained the contents of Fe, Ti, Mg, Al, Ca and Si

and their distribution characteristics. Furthermore, we worked out the global $Mg^{\#}$ values [11] and obtained the contents of FeO, TiO_2, Al_2O_5 and Mn in the lunar surface space scope of 200 m [12-13]. In addition we also obtained the distribution map of plagioclase, clinopyroxene and olivine in the whole Moon and the Aristchus impact crater, and also obtained the fully lunar distribution map of lunar space weathering degrees [14].

Based on the data acquired by the Gamma-Ray Spectrometer (GRS) onboard Chang'E-1, the relationship between radiation and topography displays different linear correlations for lunar highlands and SPA basin. It implied that the lunar highland has experienced a different evolution process from the Aitken Basin[15].

The Chang'E-2 mission succeeded in developing a key technology for material composition exploration data processing and its actual application. For example, we used the Chang'E-2 gamma spectrometer to analyze the contents of radioactive elements in large-size impact craters on the lunar surface and their adjacent ejecting materials and established the K distribution maps of the Crisium Basin and the East Sea. We also speculated the genetic mechanism of impact events[16], and we used such key technologies as X-ray spectrography data processing and inversion and obtained the data on the fully lunar distribution of Al and Mg elements, thus providing the basis for the confirmation of lunar rock types and the study of the formation and evolution of the Moon. On this basis we also established the fully lunar distribution map of U, Th, K, Fe and Al. In addition, we also observed characteristic X-ray pattern of Cr for the first time internationally, and also observed, simultaneously at one single observation time, the X-ray patterns of the following seven elements Mg, Al, Si, Ca, Ti, Cr and Fe in the region of Sinus Iridum on the Moon.

2.1.5 Near-Earth Space Environment

Based on the data acquired by the Solar Wind Ion Detector (SWID) onboard Chang'E-1 and Chang'E-2, Chinese scientists were able to identify a few interesting phenomena in the near-Moon space environment. First, the observed ion spectra reveal occasionally the presence of parallel curves, which could be interpreted as exospheric H_2^+ ions picked-up by the solar wind[17]. Second, SWID observations indicate that protons are accelerated substantially near the lunar terminator by the solar wind convective electric field and the ambipolar electric field at the flank of the lunar wake[18]. Third, the observed proton intensity approaching the well-known Lunar Magnetic Anomaly (LMA), the Serenitatis antipode, show clear signatures of depletion, deceleration, deflection as well as heating, revealing the presence of mini-magnetospheres on the Moon [19]. The solar wind ion detectors onboard Chang'E-1 recorded the solar wind Bursts of Energetic Electron (BEE) event, and its energy is positively correlated to Chang'E-1 satellite surface charging. It is further estimated that the energetic electron event would lead to the emergence of charge effect, and this may greatly influence the movement of lunar dust[20]. The interaction between the Moon and solar wind was recorded and it is the first time that the double ion beam phenomenon was found in solar wind near the Moon[21].

2.1.6 Exploration of Toutatis Asteroid

Through the analysis of morphologic features and evolution mechanism of the asteroid (Toutatis), it was revealed that the Toutatis surface was once impacted by a large number of celestial bodies. The impact crater, as large as about 800 m in diameter, in the middle-south pole region resulted from the impact of a celestial body as large as 50 m in diameter. It should be pointed out at the same time that the Toutatis is likely a rubble-pile body and its two lobes are the contact binaries [22]. It may have been formed from two independent small celestial bodies slowly closing each other, or the result of YORP effect, or the result of a large-scale impact event[23]. The flyby distance and image pixel scale were calculated from the image size of the asteroid Toutatis compared to a predicted view of an earlier radar shape model. The similarities and differences in both radar model and Chang'E-2 photo mosaic were compared, and the craters and lumps on the surface of Toutatis were measured. It was found that the density of craters on the small lobe is less than that on the big lobe (see Figure 2)[24].

3 The Main Results and Progress by Chang'E-3

The main exploration task of Chang'E-3 will be accomplished by the eight payloads on board, including panoramic camera, topography camera, descent camera, Lunar-based Ultraviolet Telescope (LUT), Extreme Ultra-Violet (EUV) camera, alpha particle X-ray spectrometer (APXS), Visible/Near-infrared Imaging Spectrometer (VNIS) and Lunar Penetrating Radar (LPR).

A total of 758 GB raw of data were received from these instruments onboard Chang'E-2.The main science results derived from Chang'E-3 were concluded as follows.

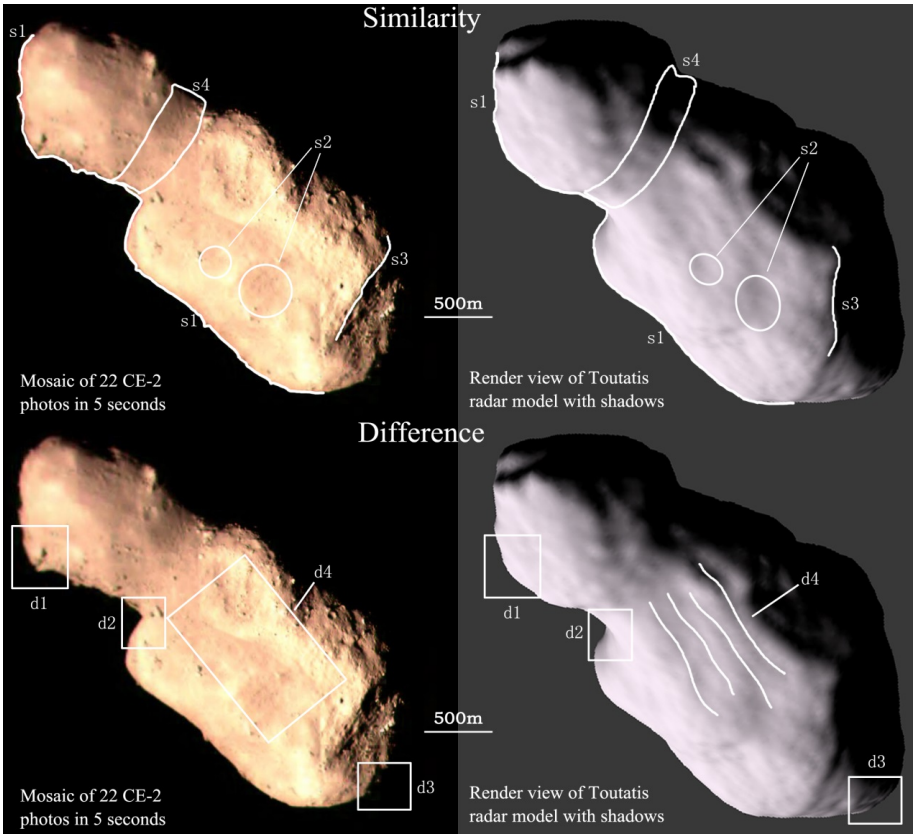

Fig.2 Comparison of the geographic features of the Chang'E-2 photo mosaic and the render frame of the radar model by Hudson and Ostro (2003). The color photos on the left are the Chang'E-2 photo mosaic, and the gray photos on the right are the render frame views with lighting of the radar model. The upper group of images shows 4 marks that indicate the similarities (s1–s4). The lower group of images shows 4 marks of the differences (d1–d4). For interpretation of the references to color in this figure legend, the reader is referred to the web version of this article

3.1 Data from the Descent Camera, the Topography Camera and the Panoramic Camera

The descent camera took 4673 pictures of lunar surface during the landing stage of Chang'E-3. The topography camera and the panoramic camera took 342 and 698 pictures of lunar surface, respectively, and the lander and rover took pictures of each other.

3.2 EUV Camera

In order to observe the Earth's plasmasphere in a global scale meridian view, a moon based EUV camera (EUVC) has been making observations at a wave band of 30.4 nm and with a field of view of 15 degrees since December of 2013. On the top deck of Chang'E-3, this camera provides images of the Earth's plasmasphere with a high angular resolution of 0.1 degrees and a temporal resolution of 10 minutes within some time intervals of moon's day during the life time of Chang'E-3 mission (probably more than one year). For this reason, we shall have many good opportunities to observe how the plasmasphere responses to solar activity and investigate behaviors of plasma in the magnetosphere.

More than one thousand of EVU images have been obtained with the EUVC. Figure 3 shows an image

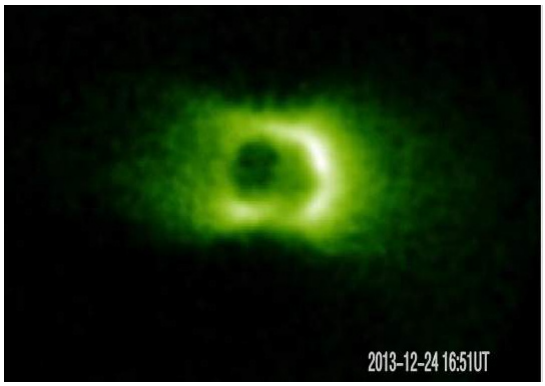

Fig.3 A preliminary result from EUVC onboard Chang'E-3. The north of the Earth is to the top side of the image, and the day side is in the right

observed at 16:51 UT on December 24, 2013. This image is a preliminary result from EUVC onboard Chang'E-3. A paper for introduction of data processing will be published in the near future. Some case studies with the EUV data during the first half of mission time are implemented in combination with some other data from ground and space based observations.

3.3 Lunar-based Ultraviolet Telescope

As a payload of Chang'E-3 mission, Lunar-based Ultraviolet Telescope (LUT) is a small telescope with a diameter of 15 cm working in near-ultraviolet band. The main scientific goal of LUT is to (1) continuously monitor variable stars without interruption for as long as more than a dozen of Earth days, (2) perform a series of low Galactic latitude sky surveys. The integrated LUT system is composed of a telescope with Ritchey-Chrétien optics, a UV-enhanced CCD detector located in the Nasmyth focus, and a pointing flat mirror configured to point to the preferred sky area.

LUT has its first light on moon at time of 02:17 (Beijing Time) in September 16, 2013. So far, it has worked on the moon for six months. The detection limit of LUT is 15.5 mag (AB system) in a nominal exposure of 30 seconds. A total of more than 50000 images were taken by LUT in the past six months. LUT has monitored eight variable stars, including eclipse double stars and RR Lyr stars, in 14 observational runs with a total of 235 hours, and surveyed a sky of more than 1000 square degrees. The obtained light curve for VW Cep taken in March 19, 2014 is shown in Figure 4. Figure 5 compares the brightness measured from LUT survey observations and that obtained from the standard stellar atmosphere models. In addition to the tight relationship between the observations and model

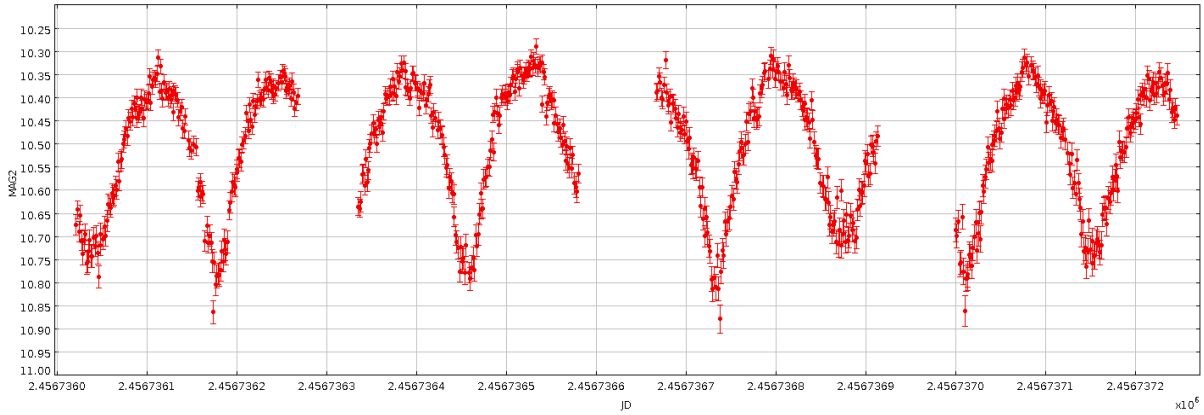

Fig.4 Light curve of VW Cep taken in March 19, 2014

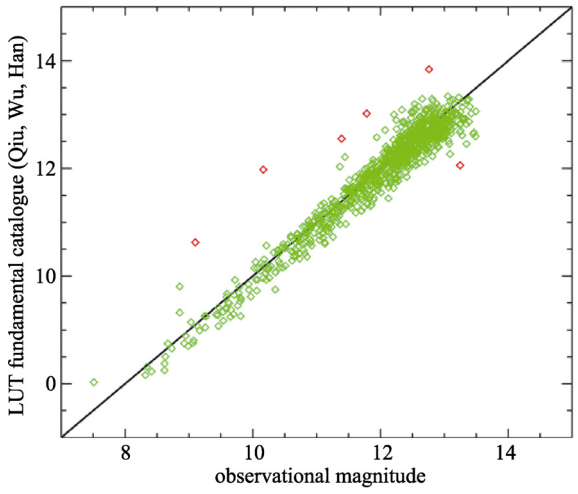

Fig.5 A tight relationship between the brightness measured from LUT observations and that estimated from standard stellar atmosphere models. The red diamonds mark the six variable stars with a deviation of more than 1 mag

expectations, a large deviation more than 1 mag can be identified for 6 variable stars.

3.4 Lunar Penetrating Radar (LPR)

LPR transmits a pulsed signal and collects echo radar signal along the path of the Yutu rover, and radar data are stored by track. The LPR started working at 10:50:32 UTC on December 15, 2013. Until April 27, 2014, the LPR worked for 8.3 hours and the traverse distance is about 109 m. 18513 and 32381 track data have been obtained for the first and second channels, respectively. Among these data, 1340 and 2531 track data are valid when LPR was walking (Figure 6). Others are repeating and similar when the Yutu rover stayed at the same place. The observations revealed that Mare Imbrium has subsurface stratifications. The depth of regolith varies from about 3 m to 10 m, and several

layers at hundreds of meters have been detected. Also the dielectric constant of the lunar top surface could be calculated and analyzed.

3.5 Alpha Particle X-ray Spectrometer (APXS)

The APXS started working at 11:05 UTC on December22, 2013. Until the end of the fifth lunar day, the APXS had worked for 5 hours and 49 minutes. The PAXS worked for detecting these elements on the lunar surface in-situ, 888 frames of EDS data and 31 frames of perception data were obtained (Figure 7).

The data acquired by the duplicated alpha particle X-ray spectrometer (APXS) on the ground and the onboard APXS have been systematically analyzed. Several background remove methods were used on a trial basis, including none background, constant background, linear background, linear polynomial background and exponential polynomial background, demonstrating that the background remove methods could significantly affect the calculated element abundances, *e.g.* Mg, Al, K, *etc*. Although the linear background could better simulate both the ground and onboard APXS data, this approach lacks a theoretical basis. Thus, further studies are still needed, *e.g.* measuring more standards, and establishing the theoretical model of the background. Preliminary data show that the measured lunar soils have high contents of Ti and Fe with 5.33 wt% TiO_2 and 20.3 wt% FeO (Figure 6).

It can be seen that the Ti/Si ratios in lunar regolith samples and their Fe/Si characteristic peak area ratios are obviously higher than those of all the measured samples. Therefore, it is hard to precisely evaluate the calculated Ti and Fe contents of lunar regolith samples, and it is also needed to make more ground calibration experiments on Ti- and Si-high samples.

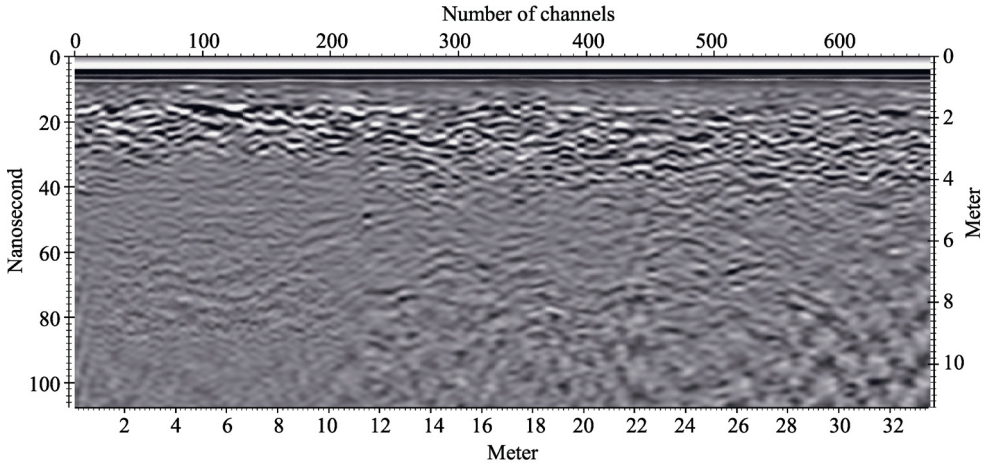

Fig.6 Primary test result of geological structure from the second channel of LPR

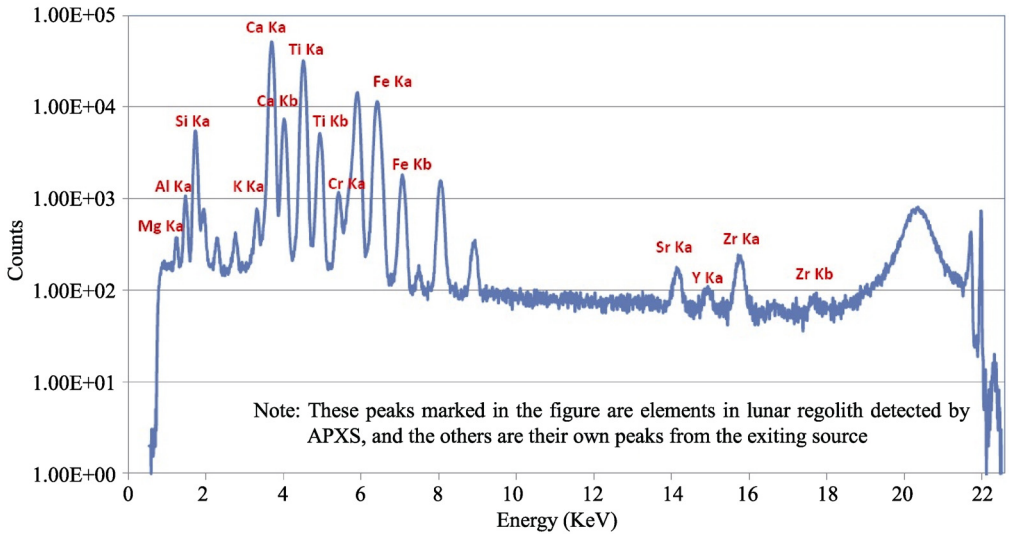

Fig.7 EDS image of the lunar regolith detected by APXS in-situ in the orbit

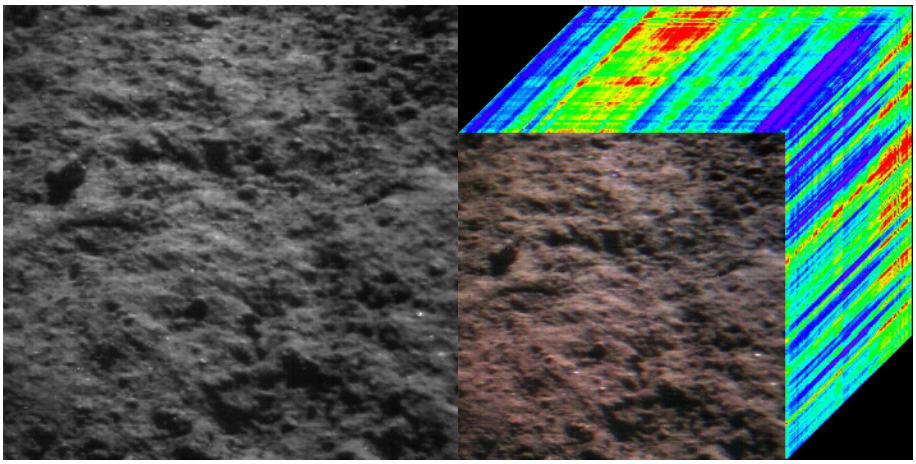

Fig.8 Single band image and its cube of VNIS's premiere lunar surface detection

3.6 Visible/Near-infrared Imaging Spectrometer (VNIS)

The VNIS started working at 10:10 UTC on December 23, 2013. Until the end of the fifth lunar day, the APXS worked for 8 hours and 46 minutes. It obtained image data of CMOS in 3360 bands and spectrometer data of SWIR in 8960 bands (Figure 8).

The VNIR reflectance spectra were extracted from VIS images and SWIR spectra based on the 2B level data, showing a typical space weathering trend as lunar mare soils. The modal compositions of pyroxene and plagioclase were decoded from the VNIR reflectance using the MGM method, with the average values of 13.8 vol% and 16.7 vol%, respectively, in consistency with those of lunar mare soils within the limit of uncertainties. The FeO and TiO_2 contents revealed by the four VNIR analyses were determined from the VIS images, varying from 13.3 wt% –16.7 wt% and 3.7 wt% –5.2 wt%, respectively. Lucey's FeO and TiO_2 algorithms were used in this work and the absolute contents calibration curves were built using lunar soils. The landing site of Chang'E-3 would be rich in TiO_2 as revealed by the APXS and VNIS data, probably representing a young lunar volcano event.

4 Summary

China's lunar exploration program has acquired a large amount of scientific data. A series of abundant scientific research results has been achieved in lunar basic science, data processing and retrieval methods, exploration of material composition, inversion of lunar soil thickness, space environment, and other scientific applications. With the deep-going work on Chang'E-3 data processing and analysis, it is believed that there will be more and more innovative scientific achievements to be made in China's lunar exploration program.

REFERENCES

[1] Wu B, Hu H, Guo J. Integration of Chang'E-2 imagery and LRO laser altimeter data with a combined block adjustment for precision lunar topographic modeling Earth Planet [J]. *Sci. Lett*., 2014, **391**: 1-15

[2] Jiang J S, Wang Z Z, Zhang X H, *et al*. China probe Chang'E-1 unveils world first Moon-globe microwave emission map the microwave Moon some exploration results of Chang'E-1 microwave sounder [J]. *Remote Sens. Tech.. Appl*., 2009, **24**(4): 409-422

[3] Zheng Y C, Tsang K T, Chan K L, *et al*. First microwave map of the Moon with Chang'E-1 data: The role of local time in global imaging [J]. *Icarus*, 2012, **219**(1): 194-210

[4] Fa W Z, Jin Y Q. A primary analysis of microwave brightness temperature of lunar surface from Chang'E-1 multi-channel radiometer observation and inversion of regolith layer thickness [J]. *Icarus*, 2010, **207**(2): 605-615

[5] Chan K L, Ksang K T, Kong B, *et al*. Lunar regolith thermal behavior revealed by Chang'E-1 microwave brightness temperature data [J]. *Earth Planet. Sci. Lett.,* 2010, **295**(1/2): 287-291

[6] Hu G P, Chen K, Huang Q L, *et al*. Brightness temperature calculation of lunar crater: interpretation of topographic effect on microwave data from Chang'E [J]. *IEEE Trans. Geosci. Remote Sens*., 2014, **52**(8): 4499-4510

[7] Zhang W G, Jiang J S, Liu H G, *et al*. Distribution and anomaly of microwave emission at lunar south pole [J]. S*ci. China: D*., 2010, **53**(3): 465-474

[8] Gong X H, Jin Y Q. Diurnal distribution of the physical temperature at Sinus Iridum area retrieved from observations of Chang'E-1 microwave radiometer [J]. *Chin. Sci. Bull*., 2011, **56**(23): 1877-1866

[9] Fa W Z, Jin Y Q. Global inventory of Helium-3 in lunar regoliths estimated by a multi-channel microwave radiometer on the Chang'E-1 lunar satellite [J]. *Chin. Sci. Bull*., 2010, **55**(35): 4005-4009

[10] Li D H, Liu H G, Zhang W G. Lunar ^{3}He estimations and related

parameters analyses [J]. *Sci. China: D*, 2010, **53**(8): 1103-1114

[11] Wu Y Z. Major elements and $Mg^{\#}$ of the moon: Results from Chang'E-1 Interference Imaging Spectrometer (IIM) data [J]. *Geochim. Cosmochim. Acta*, 2012, **93**: 214-234

[12] Yan B K, Xiong S Q, Wu Y Z, *et al*. Mapping lunar global chemical composition from Chang'E-1 IIM data [J]. *Planet. Space Sci.*, 2012, **67**: 119-129

[13] Wu Y Z, Xue B, Zhao B C, *et al*. Global estimates of lunar iron and titanium contents from the Chang'E-1 IIM data [J]. *J. Geophys Res.*, 2012, **117**:1-23

[14] Shuai T, Zhang X, Zhang L F, Wang J N. Mapping global lunar abundance of plagioclase, clinopyroxene and olivine with Interference Imaging Spectrometer hyperspectral data considering space weathering effect [J]. *Icarus*, 2013, **222**(1): 401-410

[15] Zhu M H, Ma T, Chang J. Chang'E-1 gamma ray spectrometer and preliminary radioactive results on the lunar surface [J]. *Planet. Space Sci.*, 2010, **58**(12): 1547-1554

[16] Zhu M H, Chang J, Ma T, *et al*. Potassium map from Chang'E-2 constraints the impact of crisium and orientale basin on the Moon [J]. *Sci. Reports* 2013, **3** :1611, doi: 10.1038/srep01611

[17] Wang X D, Zong Q G, Wang J S, *et al*. Detection of m/q = 2 pickup ions in the plasma environment of the Moon: The trace of exospheric H^{2+}. *Geophys. Res. Lett*., 2011, **38**: L14204

[18] Wang X D, Bian W, Wang J S, *et al*. Acceleration of scattered solar wind protons at the polar terminator of the Moon: Results from Chang'E-1/SWIDs. Geophys [J]. *Res. Lett*., 2010, **37**: L07203

[19] Wang X Q, Cui J, Wang X D, *et al*. The Solar Wind interactions with Lunar Magnetic Anomalies: A case study of the Chang'E-2 plasma data near the Serenitatis antipode [J]. *Adv. Space Res*., 2012, **50**(12): 1600-1606

[20] Wang X Y, Zhang A B, Zhang X G, *et al*. Bursts of energetic electron induced large surface charging observed by Chang'E-1 [J]. *Planet. Space Sci*., 2012, **71**(1): 1-8

[21] Kong L G, Wang S J, Wang X Y, *et al*. In-flight performance and preliminary observational results of Solar Wind Ion Detectors (SWIDs) on Chang'E-1 [J]. *Planet. Space Sci*., 2012, **62**(1): 23-30

[22] Zhu M H, Fa W Z, Ip W H, *et al*. Morphology of asteroid (4179) Toutatis as imaged by Chang'E-2 spacecraft [J]. *Geophys. Res. Lett.,* 2014, **41**(2): 328-333

[23] Huang J C, Ji J H, Ye P J, *et al*. The Ginger-shaped asteroid 4179 Toutatis: New observations from a successful flyby of Chang'E-2 [J]. *Sci. Report*s, 2013, **3**: 3411, doi:10.1038/srep03411

[24] Zou X D, Li C L, Wang W R, *et al*. The preliminary analysis of the 4179 Toutatis snapshots of the Chang'E-2 flyby [J]. *Icarus*, 2014, **229**: 348-354